Development of a vibration monitoring strategy based on cyclostationary analysis for the predictive maintenance of helicopter gearbox bearings

V. Camerini L. Macchi F. Champavier
G. Naccarato

HUMS department, Airbus Helicopters, 13725 Marignane Cedex, France

Abstract

The scope of this paper is the development of a fault detection and diagnosis method aimed to helicopter gearbox bearings vibration monitoring in an operational context. Bearings are critical components in the gearbox, and their monitoring allows for failure anticipation capabilities, leading to increased safety and improved maintenance planning. Deploying a monitoring strategy for helicopter gearboxes necessitates the development of a methodology which can provide reliable information under varying operating conditions, dealing with a noisy vibration environment and simultaneously considering acquisition system constraints, such as limited acquisition duration and sampling frequency, and operational needs, such as low rate of false alarms and minimal workload for the analyst. The approach proposed in this paper is based on the cyclostationary signals theory and relies on a two-steps procedure of detection and diagnosis. First, bearing fault detection indicators are devised on a statistical basis, leveraging on the theoretical properties of the envelope method. Then, a diagnosis based on the computation of the averaged cyclic periodogram is performed to assess the damage in the eventuality of an alarm. The developed methodology is validated on real helicopter data collected over about twenty thousand flight hours, including four bearings from different machines for which in-service spalling initiation occurred. The fault detection performance is evaluated on the basis of the achieved false alarm rates and the improvement in fault anticipation with respect to chip detectors, whereas the capability of isolating the fault-related signals using cyclostationary signal separation methods is shown for the diagnosis stage.

1 Introduction

Aircraft operations always pose the problem of guaranteeing at any time a compliant level of safety of the machine, achieved through an adequate maintenance plan, without significantly compromising its availability. In helicopters, the drive train sub-system is responsible for transferring power from the engines to the rotors, and represents a critical sub-system for the machine due to non-redundant load paths and the high variability of the dynamic loads acting on the components [1]. As to ensure aircraft airworthiness, the system needs to be maintained following a prescribed preventive maintenance program, resulting in a burden to operating costs and aircraft availability. Searching for an optimal trade-off between keeping the machine operational and reducing safety risk within acceptable hazard levels calls for making as informed as possible decisions. In the last decades, the helicopter industry worked on implementing technical solutions for increasing safety and reducing maintenance costs by enabling Condition Based Maintenance (CBM) [2, 3]. The effort resulted in the widespread adoption of Health and Usage Monitoring Systems (HUMS). Owing to the mechanical degradation of drive train components often resulting in specific vibration symptoms, and considering the widespread availability of vibration measurement systems, helicopter HUMS mostly rely on vibration analysis as a monitoring mean.

A structured breakdown of the failure mechanisms that may affect a helicopter transmission is given in [4], mostly based on [5, 6]. Failure modes may be divided into gear failure modes, bearing failure modes and shaft failure modes. From an operational point of view, the potential of vibration monitoring in driving maintenance operations toward condition based can probably at most be realized by improving the gear and bearing monitoring procedures. Gearbox inspections are expensive and require long-term grounding of the

machine. Therefore, timely detecting an impending mechanical degradation is a great advantage which results in improved maintenance planning and increased machine availability.

In this paper, a two-steps procedure for rolling element bearing fault detection and diagnosis is proposed, with the aim of obtaining a reliable operational procedure able to cope with the monitoring of a fleet of helicopters. First, cyclostationary analysis is recalled as a tool to describe and characterize the characteristic signature of a faulty bearing in section 2. Then, a procedure based on automated statistical bearing fault detection and successive fault diagnosis, and tailored on the specific features of helicopter gearbox vibration environment, is proposed in section 3. The devised strategy is validated in section 4 using data collected from a fleet of operating commercial helicopters. Finally, conclusions are drawn in section 5.

2 Theoretical background

This section is a summary of existing literature on the subject of cyclostationary methods for bearing fault detection, and does not contain original material, except for section 2.4.3.

2.1 Cyclic spectral analysis

Rotating machinery vibration signals have been in the last decades successfully modelled as cyclostationary processes [7–11]. Cyclostationarity is a property characterizing stochastic processes whose statistics vary periodically with respect to some variable (for rotating machinery, typically time or shaft's angular position) [12]. Due to this generality, it is particularly fit to describe rotating machinery signals [13]. The impact forces generated by rolling elements interacting with a local defect on the race are not repeating perfectly periodically due to slippage of the elements in normal operating conditions. Also, the transfer path to the accelerometer varies depending on the relative position of the sensor and the source of the impact. This is the case, for example, for a defect localized on any rotating element in the bearing, where the impact location varies periodically with respect to the transducer position. Such phenomena can be described by their periodic statistics, and therefore the class of cyclostationary signals is suitable to represent the associated excitation. In this paper, the second order cyclostationary descriptors are used to characterize the bearing fault signature. The main quantities of interest when dealing with cyclostationary processes in rotating machinery vibration monitoring are the cyclic spectral correlation (SC) and its normalized version, the cyclic spectral coherence (SCoh). Those quantities are bi-spectral representations, containing information related to the correlation between spectral frequency bands spaced apart by a so-called cyclic frequency α. By considering a signal $y(t)$ recorded in the time T and its Fourier transform $Y_T(f)$, its cyclic spectral correlation can be expressed as:

$$S_{yy}(f,\alpha) = \lim_{T\to\infty} E\left\{ Y_T\left(f+\frac{\alpha}{2}\right) Y_T\left(f-\frac{\alpha}{2}\right)^* \right\} \tag{1}$$

whereas the (squared magnitude) cyclic spectral coherence reads:

$$|\gamma_x(f\alpha)|^2 = \frac{|s_{yy}(f,\alpha)|^2}{s_{yy}(f+(\alpha/2))s_{yy}(f-(\alpha/2))}, \tag{2}$$

A practical estimator of the cyclic spectral correlation can be obtained using the averaged cyclic periodogram method [14]. Based on [14], the averaged cyclic periodogram for the N-length discrete sequence $x[n]$ sampled with sampling frequency F_s, computed using K (possibly overlapping) windows $w[n]$ of length N_w can be computed as:

$$\tilde{S}_{xx}^{(N)}(f;\alpha) = \frac{1}{KF_s\|w\|^2} \sum_{k=0}^{K-1} X_{N_w}^{(k)}\left(f+\frac{\alpha}{2}\right) X_{N_w}^{(k)}\left(f-\frac{\alpha}{2}\right)^*, \tag{3}$$

where:

$$X_{N_w}^{(k)}\left(f\pm\frac{\alpha}{2}\right) = \sum_{n=kR}^{kR+N_w-1} w_k[n]x[n]\mathrm{e}^{\pm j\pi wn/F_s}\mathrm{e}^{-\mathrm{j}2\pi fn/F_s} \tag{4}$$

is the DFT of the kth windowed sequence $w_k[n]x[n]e^{\pm j\pi\alpha n/F_s}$. Practically, the selection of the window length, the window function and the cyclic frequency resolution can be optimized as to minimize the computational time, minimize the cyclic leakage and find the proper trade-off between frequency resolution on the spectral axis f and variance reduction of the estimator [15]. Despite being computationally heavy, the estimator of equation (3) provides reliable results, thanks to its statistical properties, well characterized in [15]. Albeit faster algorithms were developed to estimate the cyclic spectral correlation, e.g. [16], the average cyclic periodogram method still remains a benchmark in terms of estimation accuracy and estimation variance properties.

2.2 Envelope analysis

An important relationship that can be exploited for characterizing a second order cyclostationary process is that connecting the cyclic spectral correlation of the process with its envelope spectrum. It holds from [10] that marginalizing the spectral correlation on the cyclic frequency axis, by integrating out the spectral frequency yields the squared envelope spectrum of the signal. The envelope spectrum has indeed been used in rotating machinery long before the cyclostationary framework was introduced [17]. However, the work in [10] allows to explain the efficiency of the envelope spectrum as an analysis tool for second order cyclostationary processes, framing the technique in the solid theoretical framework of cyclostationary analysis. Other than simplifying the analysis (albeit at the price of losing information on the spectral frequency distribution of the investigated process), the envelope spectrum can be easily estimated from a digitalized realization of the stochastic process by making use of the discrete Hilbert transform and the Fast Fourier Transform, and it is therefore a computationally very convenient quantity. Being equivalent to the integration of the cyclic coherence along the frequency axis, the squared envelope spectrum (SES) as a function of the cyclic frequency α, can be obtained from the N-samples discrete sequence $x[n]$ sampled with sampling frequency F_s as [14]:

$$\begin{aligned} \mathrm{ICC}_x^{(N)}(\alpha) &\propto \left|\frac{1}{N}\sum_{n=0}^{N-1}|x[n]*g[n]|^2 e^{-\mathrm{j}2\pi n\alpha/F_s}\right|^2 \\ &= \left|\mathrm{DFT}\left\{|x[n]*g[n]|^2\right\}\right|^2 \\ &= \mathrm{SES}_x^{(N)}(\alpha) \end{aligned}, \tag{5}$$

where the convolution with $g[n]$ accounts for whitening of the signal (necessary to have the power normalization leading to cyclic coherence, in place of cyclic correlation); analytic signal transformation; and band-pass filtering in a band comprised between the frequencies F_1, F_2, normally to be chosen as to filter the signal in a band in which the fault symptoms are prominent with respect to the background vibration and the interfering sources. More recently, the logarithm of the envelope spectrum (LES) for a discrete sequence $x[n]$ with $n = \{1,...,N\}$ was introduced in [18] as:

$$LES_x[\alpha] = \left|\frac{\sum_{n=0}^{N-1}\log\left(x[n]^2\right)e^{-2\pi jn\alpha/F_s}}{N}\right|^2, \tag{6}$$

The LES is an interesting quantity to be considered in an automated detection framework, thanks to its advantageous statistical properties demonstrated in [18].

2.3 Statistical tests for cyclostationarity

The problem of detecting the second order cyclostationarity is formulated as the decision between the two alternative hypotheses:

$$\begin{aligned} &\mathrm{H}_0 : \text{"The signal does not contain a CS2 component at the cyclic frequency } \alpha\text{"} \\ &\mathrm{H}_1 : \text{"The signal contains a CS2 component at the cyclic frequency } \alpha\text{."} \end{aligned} \tag{7}$$

2.3.1 Testing the SES for cyclostationarity

A rigorous statistical test for the presence of a cyclostationary component at frequency α was given in [14] and is based on the cyclic coherence. By exploiting the link between the cyclic coherence and the SES, a practical statistical test on the SES can be obtained, with the advantage of allowing to work on a simpler, faster

to compute quantity. Namely, for a discrete signal $x[n]$ of length N, the following result is obtained in [14] by extending the statistical test on the cyclic coherence, and in [19] following a direct analysis of the discrete SES:

$$\text{"Reject } H_0 \text{ if:"} \text{SES}_x^{(N)}(\alpha) \geqslant \frac{\sigma_{x*g}^4}{2N} \frac{F_s}{F_2 - F_1} f(\alpha) \cdot \chi_{1-p,2}^2\text{"}, \tag{8}$$

being p the significance level of the test, σ_{x*g} the standard deviation of the filtered signal $x[n] * g[n]$ and:

$$f(\alpha) = \begin{cases} 1 - |\alpha| / (F_2 - F_1), & |\alpha| < F_2 - F_1 \\ 0 & \text{elsewhere} \end{cases} \tag{9}$$

It is important to underline that the optimality of the test is obtained under the assumption of white noise signal for a healthy component. An analysis of the effects of CS1, CS2 components and colored noise on the SES of the signal is exhaustively performed in [19]. The relevant points are summarized below:

- The effects of a set of M additive multi-harmonic CS1 components of frequencies λ_m, $m = \{1, ..., M\}$ are that of biasing the SES at the difference frequencies $\{\Delta\lambda\} = \{\lambda_m - \lambda_n\}$, $m, n = \{1, ..., M\}$; and that of amplifying the variance in large frequency bands.
- The effect of an additive CS2 component in the signal is that of introducing a bias in the estimator of the SES, which is stronger when the average power of the CS2 carrier is dominating over the background noise.
- The generalization to colored noise implies estimating the variance of the signal at each frequency bin, resulting in a statistical threshold which is no longer a linear function of the frequency.

2.3.2 Testing the LES for cyclostationarity

For a white noise, discrete signal $x[n]$ of length N, the distribution of the LES at a cyclic frequency α is given in [18] as:

$$\frac{\text{LES}_x[\alpha]}{\pi^2/4N} \sim \chi_2^2 \tag{10}$$

Therefore, the LES test for cyclostationarity at significance level p reads:

$$\text{"Reject } H_0 \text{ if:"} \text{LES}_x^{(N)}(\alpha) \geqslant \frac{\pi^2}{4N} \cdot \chi_{1-p,2}^2\text{"}, \tag{11}$$

The LES allows estimating the CS2 components in the signal with the following advantages with respect to the SES:

- The estimator is unbiased by the presence of cyclic components of a frequency different than the considered one.
- Under the white noise assumption, the variance of the estimator is independent from the variance of the noise in the signal.

The second point is more a matter of mathematical rigor for long, whitened noise signals, whereas the first point constitutes an important advantage of the LES when it comes to defining automated tests for the presence of cyclostationary components at a frequency of interest. Additionally, the LES was shown to yield better statistical performance in presence of impulsive noise [20]. This last characteristic is not surprising in light of its being unbiased from CS2 components, considering the existing relation between the CS2 components in the signal and its Kurtosis [21].

2.4 Signal pre-processing

In order to leverage on the optimality of the statistical tests discussed in section 2.3, it is necessary to bring the analyzed signal's statistics as close as possible to the white noise conditions. First, it is a good practice to remove CS1 components from the signal, as they have a biasing effect as explained in section 2.3. The removal of CS1 components can be performed, e.g., through estimation and subtraction. Such an estimation can be performed in different ways, depending on whether the fundamental cycle of interest is known or not. In the case it is not, it can be based on blind estimators, as the linear adaptive enhancer (ALE), or the self-adaptive noise canceller (SANC) and its more efficient frequency domain formulation [22–25]. Generally, blind estimators performance is negatively affected by signal to noise ratio. Moreover, blind filters require a proper parameter tuning which may not be trivial in every case. When the cycle of the signal is known, a popular estimator of the periodic mean is the synchronous average (SA) operator, which is also known as Time Synchronous Average (TSA) due to its original formulation in time domain [26]. In order to obtain the periodic mean in the case of a quasi-cyclostationary signal, the SA must be applied for each of the fundamental cycles which are present in the signal, and then the extracted periodic components need to be summed together [13]. Once the deterministic part of the signal is removed, it is necessary to obtain a flat frequency spectrum for the signal, resembling white noise statistics. In order to do so, there are mainly two strategy: one is selecting a narrow-band frequency region and filter it out; the other is to apply any method to "flatten" the spectrum, such as cepstrum pre-whitening (CPW) [27–29]. On the other hand, the estimation bias resulting from the exogenous CS2 components discussed in section 2.3 cannot be simply corrected for, due to its statistical nature. As a summary, two main steps shall be performed before analyzing the signal, i.e. removal of CS1 components and pre-whitening of the residual. In this work, two techniques were found particularly useful for the scope: the angular domain synchronous average and the cepstrum pre-whitening. The first technique is preferred as the cycles of the main additive deterministic components are known for a given gearbox, whereas the second one is preferred over filtering, as it allows to consider the full-band signal in the analysis, avoiding a further optimization step to select a narrow-band filter which is able of isolating the fault signature (e.g., Spectral Kurtosis [30] is a popular tool that can be used for the scope). Also, if compared to other pre-whitening techniques, the CPW excels for the simplicity of use and the lack of configuration parameters to be properly selected.

2.4.1 Synchronous average removal

Under the assumption of cycloergodicity [13], SA is indeed a practical estimation of the periodic mean of a CS signal, which is its first order cyclostationary part of cycle equal to the fundamental period used for averaging. The equation for the SA of a signal $x(\theta)$ of fundamental cycle Θ reads in angle domain [31]:

$$SA[x(\theta)]_\Theta = \frac{1}{N}\sum_{i=0}^{N-1} x(\theta + i\Theta) \tag{12}$$

Synchronous averaging is thus equivalent to applying a comb filter to the signal [13], which extracts the multiples of the reference harmonic. The number of averages controls the bandwidth of the lobes, the amount of noise rejection and the position of the notches of the filter. In order to remove multiple cycles linked to different harmonic families, equation (12) can be applied multiple times to extract the harmonic family of interest and then subtract it from the original signal. It is worth mentioning that an "order tracking" or "angular resampling" step has to be performed to correct for small speed fluctuations, expressing therefore the measured vibration signal in the angle-domain form of equation (12) [27]. This angular resampling step is typically performed using a synchronization signal acquired from an external measurement system, as e.g. a magnetic pick-up sensor mounted on a reference shaft [31].

2.4.2 Cepstrum pre-whitening

The pre-whitening operation consists in setting a zero value for the whole real cepstrum (except possibly at zero quefrency), then, once transformed back to the frequency domain, the obtained signal is recombined with the phase of the original signal and inverse transformed to time domain [29]. Considering a signal x, its

pre-whitened version can be simply computed as [29]:

$$x_{cpw} = IFT\left\{\frac{FT(x)}{|FT(x)|}\right\} \tag{13}$$

2.4.3 Remarks on signal pre-processing

The two steps of signal pre-processing carry with them some hidden difficulties which is worth pointing out. First, it is necessary to observe that the synchronous average removal requires angular resampling of the signal, and when it is performed using the computed order tracking (COT), it involves interpolating the signal in order to obtain its angle-domain values. In [32], a discussion of interpolation methods is given. Interpolating acts as a low-pass filter in the frequency domain. Therefore, it is important to keep into account that any order tracking step has the effect of distorting the signal's spectrum by attenuating the high-frequency components. As a consequence, spectral flattening shall always be performed after order tracking, when envisaging the use of the statistical tests of section 2.3. Furthermore, the cepstrum pre-whitening enhances the sensitivity of the squared envelope results to phase correlation. This last issue is formalized below by using a simple, unit amplitude complex harmonic signal as an example. Consider the following:

$$x(t) = e^{j2\pi\tilde{f}t} \tag{14}$$

then its Fourier transform reads:

$$X(f) = \delta(f-\tilde{f}) \tag{15}$$

being $x(t)$ complex analytic, and noting $\overline{x}(t)$ its complex conjugate, then the envelope spectrum can be computed as:

$$\mathrm{ENV}_x(f) = FT(x(t)\cdot\overline{x}(t)) \tag{16}$$

if a finite-length, discrete signal $y[n] = x[n]\cdot w[n]$, $n = \{1,...,N\}$ is considered (neglecting the sampling step from the notation for simplicity), being $w[n]$ a rectangular, causal observation window of length N, and the Discrete Fourier Transform is used to compute the Fourier transform, it holds:

$$\mathrm{ENV}_y[k] = \frac{1}{N}\sum_{n=0}^{N-1} y[n]\cdot\overline{y}[n]\cdot\exp\left(-j2\pi\frac{nk}{N}\right) \tag{17}$$

then by the convolution theorem, equation (17) can be rewritten as:

$$\mathrm{ENV}_y[k] = \sum_{r=k}^{N/2} Y[r]\cdot\overline{Y}[r-k] \tag{18}$$

again, for the convolution theorem, the sifting property of the Dirac's delta distribution $\delta(\cdot)$, and considering the Fourier transform of the rectangular window $w[n]$, equation (18) can be expressed as:

$$\mathrm{ENV}_y[k] = \sum_{r=k}^{N/2}\frac{\sin(\pi(r-\tilde{k}))}{\sin(\pi(r-\tilde{k})/N)}e^{-j\pi(r-\tilde{k})\frac{N-1}{N}}\cdot\frac{\sin(\pi(r-k-\tilde{k}))}{\sin(\pi(r-k-\tilde{k})/N)}e^{j\pi(r-k-\tilde{k})\frac{N-1}{N}} \tag{19}$$

where $\tilde{k}$ denotes the discrete frequency index corresponding to $\tilde{f}$. After the cepstrum pre-whitening operation of equation (13), only the phase terms are left from the DFT of the original signal and equation (19) becomes:

$$\mathrm{ENV}_y[k] = \sum_{r=k}^{N/2} e^{-j\pi(r-\tilde{k})\frac{N-1}{N}}\cdot e^{j\pi(r-k-\tilde{k})\frac{N-1}{N}} = e^{-j\pi k\frac{N-1}{N}}(\frac{N}{2}-k) \tag{20}$$

From equation (20), it can be observed that the phase correlation from residual periodic components has a harmful effect on the classical envelope spectrum of the pre-whitened signal, which is amplified when the amplitude spectrum of the signal is equalized to the unit value.

2.5 Bearing fault signature

Healthy bearings vibration does not typically bring a significant contribution to the vibration generated by a helicopter gearbox. On the other hand, a defective bearing generates a characteristic vibration signature, characterized by repeated impacts occurring each time that a bearing element contacts the defective surfaces [5, 33–35]. Typically, four characteristic frequencies can be identified: ball pass frequencies on the outer and inner races (respectively BPFO and BPFI), typically linked to localized defects on one of the races; fundamental train frequency (FTF), generally linked to cage defects; and ball spin frequency (BSF), normally related to localized defects on the rolling elements surface. By indicating with f_i and f_e respectively the inner and outer race rotation frequency, with N_b the number of rolling elements in the bearing, by α_0 the initial contact angle, by d the rolling element diameter and by D the bearing pitch diameter, these characteristic frequencies read [36]:

$$\begin{aligned} BPFI &= \frac{N_b\,|f_e - f_i|}{2}\left(1 + \frac{d}{D}\cos(\alpha_0)\right) \\ BPFO &= \frac{N_b\,|f_e - f_i|}{2}\left(1 - \frac{d}{D}\cos(\alpha_0)\right) \\ BSF &= \frac{D\,|f_e - f_i|}{2d}\left(1 - \left(\frac{d}{D}\cos(\alpha_0)\right)^2\right) \\ FTF &= \frac{1}{2}\left(f_e\left(1 + \frac{d}{D}\cos(\alpha_0)\right) + f_i\left(1 - \frac{d}{D}\cos(\alpha_0)\right)\right) \end{aligned} \tag{21}$$

Letting $h_j(t)$ be the impulse response to a single impact measured by the sensor located at position j, $q(t)$ the periodic modulation owing to load distribution (or periodic changes in the loading conditions, or sensor orientation/position with respect to the impact point) [37, 38], and letting T be the fundamental impact periodicity (which can be computed by inverting the frequency of interest from equation (21)); then the measured response $x_j(t)$ related to the defective bearing was given in [14, 39–41] as:

$$x_j(t) = \sum_{i=-\infty}^{+\infty} h_j(t - iT - \tau_i)\, q(iT) A_i + n_j(t), \tag{22}$$

where $n_j(t)$ includes the additive background noise and all eventual interference sources, the subscript i indicates the ith impact, τ_i represents the mentioned uncertainty on pulse arrival time and A_i the random amplitude of the impact. Both the variables are modeled in [14] as mutually independent, white, stationary random sequences with respectively zero and unity mean. Those idealized assumptions allow, according to the literature, to gain sufficient insight into the described phenomenon. The fault signature appears as a pseudo-periodic excitation consisting of pulses which are separated by a period close to that of the fault frequency, but affected by a small, random variation typically of the order of one percent of the fundamental period. Such slight fluctuations results practically in destroying the discrete, harmonic structure that would arise if the random fluctuations were neglected as in [34], giving raise to an essentially random vibration signal in the frequency range of interest [14]. The main difference between the model found in [34] and that of equation (22) is that in the latter, the harmonic structure produced by the fault-related impacts rapidly turns into a random signal. As a consequence, the bearing fault signature in the spectrum is likely to be localized in the low-frequency region, and therefore subject to masking from the background noise and from other possibly existing interference sources, as e.g. gear mesh harmonics. Hence, the model can explain the reason for which classical spectral analysis may fail in detecting rolling-element bearing faults, making this signal representation closer to the reality of the phenomenon. A practical solution to this issue resides in making use of the second-order cyclostationary tools presented in section 2.1 in order to isolate the bearing vibration signature from the rest of the measured signal. The cyclostationary approach was actually shown very successful for bearing diagnostic problems in several works, as in [10, 14, 19, 21, 33, 41]. From equation (1), adopting the proper normalization to obtain the cyclic power spectrum from the spectral correlation, it can be shown that for the signal model of

equation (22), it holds [10]:

$$S_{x_j}(f,\alpha) \simeq \frac{1}{T} H_j\left(f+\frac{\alpha}{2}\right) H_j\left(f-\frac{\alpha}{2}\right)^* \left(\Phi(\alpha)\left(1+\sigma_A^2\right) - \Phi\left(f+\frac{\alpha}{2}\right)\Phi\left(f-\frac{\alpha}{2}\right)^*\right) \times \sum_{k,l=-\infty}^{+\infty} Q_l \delta\left[\alpha - \frac{k}{T} - \frac{l}{P}\right] + \delta[\alpha] S_n(f) \quad , \tag{23}$$

in which $\Phi(f)$ stands for the Fourier transform of the probability density function of the random variable τ associated to the impacts jitter, P for the load variation characteristic period, $H_j(f)$ for the transfer function from the impact point to the measurement location j, obtained as the Fourier transform of the impulse response function $h_j(f)$, σ_A the standard deviation of the random variable A representing the random impact amplitude, and the Q_l are coefficients of the Fourier transform of the modulating function $q(t)$. The weak harmonic contribution was neglected, being it highly attenuated in the high frequency region as an effect of the random jitter of the impact times. From equation (23), the discrete structure of the bearing signature is finally evident in the cyclic power spectrum plane, with continuously distributed values along the spectral frequency lines appearing at multiples of the fundamental impact frequency (along axis α). Also, the values are higher for those spectral frequency bands where the fault signature is dominating. It follows for the cyclic coherence [14]:

$$\left|\gamma_{x_j}(f,\alpha)\right|^2 \simeq \left|\frac{\mathrm{SNR}(f)}{1+\mathrm{SNR}(f)}\right|^2 |\Phi(\alpha)|^2 \sum_{k,l=-\infty}^{+\infty} \left|\frac{Q_l}{Q_0}\right|^2 \delta\left[\alpha - \frac{k}{T} - \frac{l}{P}\right], \tag{24}$$

where $SNR(f)$ represents the signal-to-noise ratio of the fault. Consequently, as a function of the spectral frequency f, equation (24) shows an increased coherence for increasing amplitude modulation randomness, impact frequency and load modulation intensity, whereas as a function of the cyclic frequency α, it shows a discrete structure consisting of harmonics of the fault signature separated by the characteristic impact frequency, with decreasing amplitude depending on the low-pass filtering function $\Phi(\alpha)$. Therefore, the highest the multiple of the fundamental impact frequency, the lower the intensity of the observed bearing signature in the cyclic coherence. Equation (3), along with the proper normalization, can be used to estimate the quantity appearing at the LHS of equation (24), yielding an efficient diagnostic representation able of highlighting the bearing fault signature according to the structure of equation (24).

3 Proposed monitoring procedure

Operationally, it is desirable to control the risk of false alarms from the health monitoring system, in addition to providing the earliest possible warning. In order to achieve those targets, a two-steps procedure is proposed in this work. First, statistical indicators leveraging on the cyclostationary theory are designed in order to attain a specified false alarm rate. Secondly, a diagnostic step based on the analysis of the cyclic coherence is taken each time that an alarm is raised, in order to confirm that the threshold exceedance is actually due to a mechanical defect. The importance of the first step of the procedure is that of providing an easy-to-read scalar indicator, with known statistical behavior, which can be employed to guarantee a given false alarm rate as low as not to overload the analysts, maintaining contextually an acceptable detection performance. The second step implies confirming the alarms raised in the detection phase before performing any maintenance, as a measure to avoid unnecessary grounding of the concerned helicopters.

3.1 Fault detection stage

With the aim of deriving statistically reliable monitoring indicators, the cyclostationary signal theory is adopted in this work within the frame of a procedure similar to that proposed in [42]. The envelope spectrum is here computed through the methods described in section 2.2. Both SES and LES can be considered. The necessity of an automated bearing monitoring gives raise to the following challenges:

1. The false alarm rate shall be kept under control in order to avoid unnecessary grounding of the machine;
2. The actual fault frequency cannot be accurately predicted using the simplified kinematics relations;
3. Interfering, exogenous components may mask the bearing fault signature.

As to cope with the first point, the statistical tests presented in section 2.3 for LES and SES can be exploited. First, a signal pre-whitening step consisting of the removal of the periodic (CS1) components through synchronous averaging followed by cepstrum pre-whitening for spectral flattening is performed. This allows to get rid of interferring CS1 sources and to bring the signal's statistics closer to those of white noise. A statistical threshold can then be derived from the white-noise envelope spectrum statistics as in [18, 43]. For a number of bearing fault harmonics to be configured, a narrow-band frequency range around the fault frequencies of an extent to be configured, can be defined. This is done in order to allow some margin in considering eventual shifts of the fault frequency from its predicted nominal value, addressing the second problem in automatizing the algorithm. At the same time, if the considered cyclic frequency range is too wide, there is the risk of exogenous CS2 components leaking into the analysis band, leading to incorrect diagnosis. This issue has to be carefully addressed when tuning the algorithm's parameters. Any number of fault harmonics can be considered in the algorithm. However, according to equation (24), best results are obtained for the low bearing harmonics. For each defined range, the values of the SES or LES are compared to the statistical thresholds of equations (8) and (11). If any statistically significant value is present, a fault detection alarm is raised. The advantages of the adopted procedure are two-fold: on one hand, the envelope spectrum is computed in a computationally efficient way; on the other hand, the computation of the theoretical threshold after pre-whitening according to [18, 43] provides solid grounds for statistical testing. For a given signal to be processed, the algorithm can be summarized in the following steps:

1. Define the desired false alarm rate $P\tilde{F}A$ for the indicator according to the operational needs;
2. Calculate the fault frequency of interest F_F (according to equation (21)) in units of the sampling frequency F_s;
3. Set the number of fault harmonics N_h to be monitored;
4. Set a tolerance band ψ as a percentage of the fault frequency of interest, in order to account for the uncertainty on the actual fault frequency;
5. Remove known CS1 components using synchronous average removal;
6. Apply spectral flattening using cepstrum pre-whitening;
7. Compute the full-band SES/LES of the pre-whitened signal;
8. Compute the statistical threshold p according to the defined desired false alarm rate, based on the white noise assumption;
9. For each considered fault harmonic: find the maximum value of SES/LES in the defined tolerance band;
10. Compute the indicator value as the mean of the statistically significant values with respect to the defined threshold (if no significant value is found for any of the considered harmonics of the fault, the indicator value is set to zero).

The expected false alarm rate $P\tilde{F}A$ corresponds to the probability of one value of the (squared or logarithmic) envelope spectrum within the considered range being higher than its statistical threshold computed through equations (8) and (11). Therefore, to attain a desired level for $P\tilde{F}A$, it is necessary to calculate the significance level p as to satisfy:

$$P\tilde{F}A = 1 - p^{\sum_{h=1}^{N_h} r_h} \tag{25}$$

with N_h being the number of the considered fault harmonics and:

$$r_h = \lceil h \frac{\psi}{100} \frac{F_F}{F_s} N \rceil \tag{26}$$

where N is the discrete signal length and F_s its sampling frequency expressed in inverse units of the sampling step. The value of p obtained from equation (25) allows for calculating the statistical thresholds of equations (8) and (11) so that the probability of having one exceedance of the envelope spectrum in the computational range is equal to $P\tilde{F}A$. It is important to point out that where the false alarm rate can be kept under control, the detection performance cannot be predicted a priori. Typically, the higher the tolerance band ψF_f, the lower the detection performance for a fixed $P\tilde{F}A$; the higher the admissible alarm rate $P\tilde{F}A$, the higher the detection performance that can be expected.

3.2 Fault diagnosis stage

Each time an alarm is triggered, a fault diagnosis step is performed by the analyst. It consists of computing the cyclic spectral coherence around the fault frequencies for which the detection algorithm raised an alert and visually assessing the existence of CS2 components compatible with the expected signature from a bearing fault. The spectral coherence is estimated according to equation (3), where the number of averages and the window length are set according to the guidelines discussed in [15]. Within this assessment step, the analyst can additionally assess the presence of diagnostic side-bands carrying supplementary information on the nature of the fault.

4 Results

In this section, the proposed monitoring strategy is applied on in-service helicopter HUMS data in order to assess its performance in terms of reliability and detection. LES and SES indicators, along with different pre-processing treatments are compared, stressing the importance of properly pre-whitening the signal before carrying on with the analysis.

4.1 Data description

In order to validate the proposed procedure, a comprehensive data-set consisting of vibration data recorded from fourteen machines over about twenty-thousand flight hours (FH) is considered. The data-set includes four bearing in-service degradation cases that were detected by the HUMS: two of them concern roller bearings, and the other two concern ball bearings. The acquisitions were performed in various operating conditions, involving different regimes for the rotational speed of the rotor and for the transmitted torque from the engines. Main gearbox (MGB) and accessory gearbox (AGB) acquisitions comprise signals from seven accelerometers and two keyphasor signals. The two keyphasor signals provide respectively one pulse per revolution of the main rotor and of the tail rotor shaft. Accelerometers are typically mounted on the gearbox casing, close to the monitored components. Generally, acquisitions are divided in groups. Each acquisition group is launched when specific flight conditions are matched and consists of a synchronized acquisition from a set of sensors, performed with a configured sampling frequency for a configured duration. The available keyphasor signals are always sampled with the same sampling frequency of the accelerometer signals. Signals were sampled synchronously from all the MGB accelerometers with a sampling frequency of 50 kHz, for one second duration. The four documented bearing fault cases occurred on different machines during the monitoring period. The faults were anticipated by the HUMS in the spalling initiation phase, allowing for timely maintenance. Table 1 summarizes the four selected fault cases, whereas figure 1 show the inspected bearings after component removal. All the cases involve outer race spalling which occurred whether on a roller or on a ball bearings. The HUMS, through the deployed monitoring strategy, triggered regular inspections of the chip detectors and allowed in each case to anticipate the chip warning coming from the oil metal chips detectors. Additionally, for the fault case 4, HUMS had gained enough confidence to trigger the removal without the need of waiting for the metal particles in the chip detector to be out of criteria. The geometrical parameters of the concerned bearings are not reported for proprietary reasons.

Table 1 – Fleet selected bearing fault cases summary

Fault case ID	Machine ID	Damaged bearing
1	1	Roller bearing (bearing 1)
2	2	Roller bearing (bearing 1)
3	3	Ball bearing (bearing 2)
4	3	Ball bearing (bearing 2)

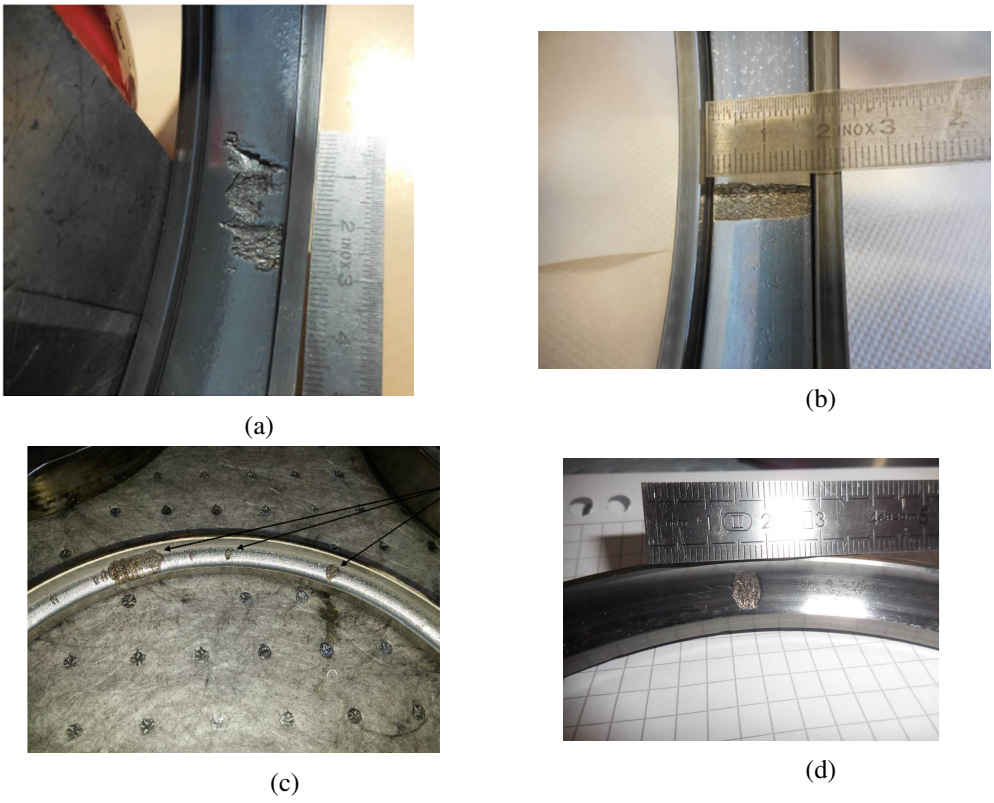

Figure 1 – Damaged bearings after inspection. Outer race presenting spalled area at the time of removal – a) Bearing fault case 1 ; b) Bearing fault case 2; c) Bearing fault case 3 ; d) Bearing fault case 4.

4.2 Fault detection performance

The bearing monitoring strategy proposed in section 3 is applied on the operational data of this section. Bearing anomaly indicators are computed routinely on all the fleet data, and then the detected exceedances are analyzed using cyclostationary analysis in order to complete the diagnosis. Although bearing anomaly indicators are computed for each monitored bearing in the gearbox, the results here presented are restricted to those for which the faults were observed, allowing to validate both detection and the reliability performance. From the bearing geometrical properties, the theoretical characteristic frequencies could be computed according to equation (21). Table 2 reports the computed, nominal bearing defect frequencies for the considered bearings 1 and 2, expressed in orders of the rotational speed of the shaft to which they are attached. According to the nominal design parameters, the fault frequencies are very close (for the outer race defect frequency, the difference between bearing 1 and 2 is less than two percent), posing a challenge in discriminating which one is the faulty bearing in the event of a detection. Both SES-based and LES-based indicators are evaluated, computing the envelope spectra on the pre-whitened signal after a synchronous average removal step and cepstrum pre-whitening (SES-CPW and LES-CPW indicators). Performance on the signal after the synchronous average removal step only are also reported for comparison (SES-SA and LES-SA indicators). The indicators were configured such as to allow to separate the two fault frequencies, but allowing some slippage through one-percent width analysis bands. Only the first harmonic of the outer race fault frequency was considered. With reference to section 3, care was taken when performing the OT steps in the SA removal and when resampling the signal to order domain before the cepstum pre-whitening.

Table 2 – Bearing 1 and 2 characteristic fault frequencies in order domain.

Parameter	Description [dimension]	Bearing 1 Value	Bearing 2 Value
BSF	Roller Spin Frequency [Hz]	3.64	3.67
FTF	Fundamental Train Frequency [Hz]	0.44	0.45
$BPFO$	Ball Pass Frequency Outer race [Hz]	9.69	9.85
$BPFI$	Ball Pass Frequency Inner race [Hz]	12.31	12.15

Figure 2 shows the actual false alarm rate against the expected one for the SES and LES indicators for bearing 1 and bearing 2 on the whole collected healthy fleet data. It can be seen that the actual alarm rates for both the bearings do not match well the expected results in the case of the SA indicators. This is attributable to two main factors: first, the SA procedures do not remove all of the periodic components originally present in the signal, leaving some residual, biasing CS1 component; secondly, the spectrum of the measured vibration is far from resembling white noise, leading to the statistical thresholds computed using equations (8) and (11) being inaccurate. On the other hand, figures 2c and 2d show better results for the indicators computed after the cepstrum pre-whitening step. From the distribution check it can be seen that the LES-based indicator provides very accurate results for both the considered bearings: the actual false alarm rate agrees very well with the predicted one. Conversely, despite the spectral flattening and the SA removal, the SES indicator yields higher false alarm rate than expected. This fact might be explained by the SES statistics being affected by exogenous CS2 components, differently from those of the LES. In order to evaluate the detection performance of the devised statistical indicators, an anticipation over removal metrics is introduced. For each fault case, the removal anticipation (RA) achieved by HUMS alert and expressed in acquisitions number, was computed as a function of the actual false alarm rate on the fleet. Typically, the removal is triggered by an inspection of the particles captured in the chip detector and matching some criteria on size and composition. The RA figure allows to judge the achievable trade-off between detection capability and global false alarm rate performance of an indicator. Figures 3a and 3b show the results respectively for the fault cases 1 and 2, for the SES-SA and LES-SA outer race fault indicators, whereas figures 4a and 4b report the same results for the SES-CPW and LES-CPW outer race fault indicators. Concerning the fault cases 3 and 4, related to the ball bearing, the RA is constant for each considered indicator, despite pre-processing differences and equal respectively to 66 acquisitions and 34 acquisitions. This depends actually on two distinct facts: first, in the considered data-set, acquisitions for machine 3 begins already in a relatively advanced bearing degradation stage, where all indicators detect very clearly. Secondly, the second degradation produced very early, strong CS2 symptoms which were as well detectable in a robust manner from all of the considered indicators. Also, for the second ball bearing degradation (fault case 4), the HUMS alerting system was already deployed, and guaranteed the detection of the incipient bearing degradation, along with an optimized, planned maintenance intervention. Therefore, the time to removal metrics is not representative of the anticipation over the chip detector alert for case 4. For the roller bearing degradation cases, evidently the SES-CPW and LES-CPW achieve a better anticipation over removal for a given false alarm rate, implying their better performance in terms of early detection with respect to the SES-SA and LES-SA indicators in both the cases. The comparison between LES-CPW and SES-CPW shows that they perform very similarly for the first fault case (figure 4a), whereas the SES-CPW indicator shows better detection performance with respect to the LES-CPW in the second fault case (figure 4b).

4.3 Fault diagnosis stage

In this section, the diagnostic charts based on the cyclic coherence are shown for each detected bearing degradation. The defined operational procedure only requires to compute such quantities when an alert is raised, so to confirm the actual occurrence of a mechanical degradation. In figures 5 to 8, for fault cases respectively 1 to 4, the diagnostic charts and the associated LES and SES spectra, together with their statistical threshold computed for the 0.1 percent significance level according to equations (8) and (11), are shown in three conditions: before the beginning of the bearing degradation, during the bearing degradation and after gearbox replacement. In each case, the spalling manifests as a high-frequency excitation, at a cyclic order which is slightly different than that predicted from the theoretical calculations. Consequently, the actual loading conditions encountered in operations have an impact on the exact determination of the fault frequency, owing to the simplified kinematics assumptions being inadequate to describe the bearing dynamic behavior. By comparing figure 5 to figure 6, it can be seen that the symptoms of the spalling appears much more evident for the second fault case (compare, e.g., the statistical threshold to the value of the emerging peak in the two cases). Coherently, figures 3 and 4 show that the second fault case is predicted with a higher anticipation time from both the SES and LES indicators. This can be explained by looking at figure 1. It can be noticed from figure 1a and figure 1b that the shape of the surface degradation is consistently different in the two cases. In fault case number 2, the spalling area extends across the full span of the race, creating a slot. Conversely, in fault case number 1 the spalling area is restricted to part of the width of the race. It can be expected that for the second degradation

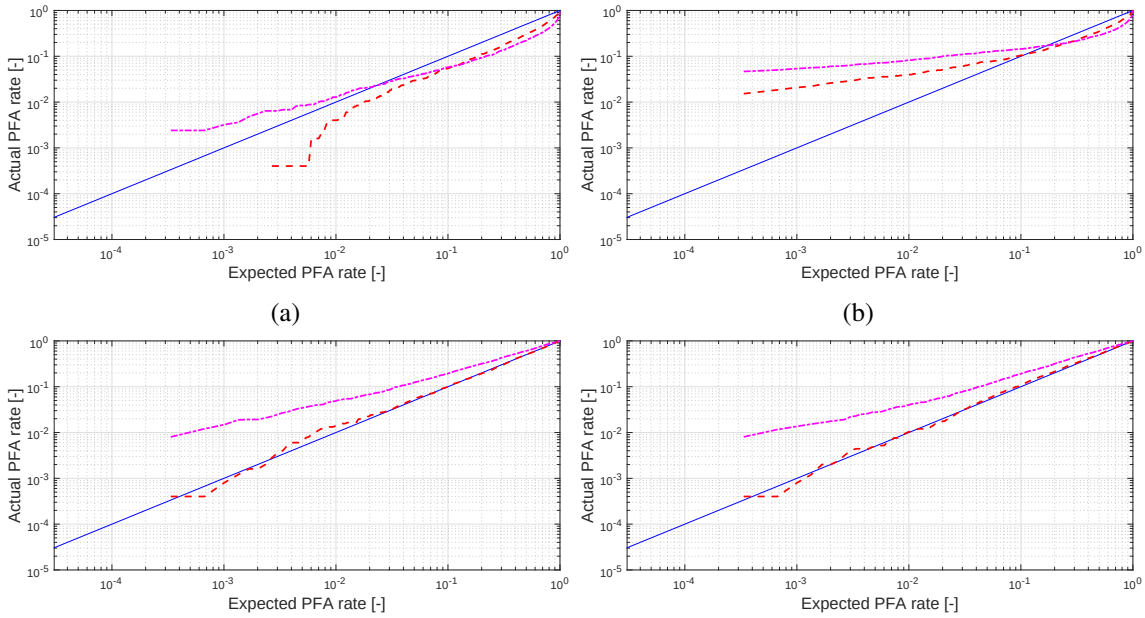

Figure 2 – Healthy fleet data, actual vs. expected probability of false alarm rate of the SES and LES outer race fault detection indicators for: a) Bearing 1, SA indicators; b) Bearing 2, SA indicators; c) Bearing 1, CPW indicators; d) Bearing 2, CPW indicators. Blue: theoretical relation; red dashed: LES indicator; magenta dot-dashed: SES indicator.

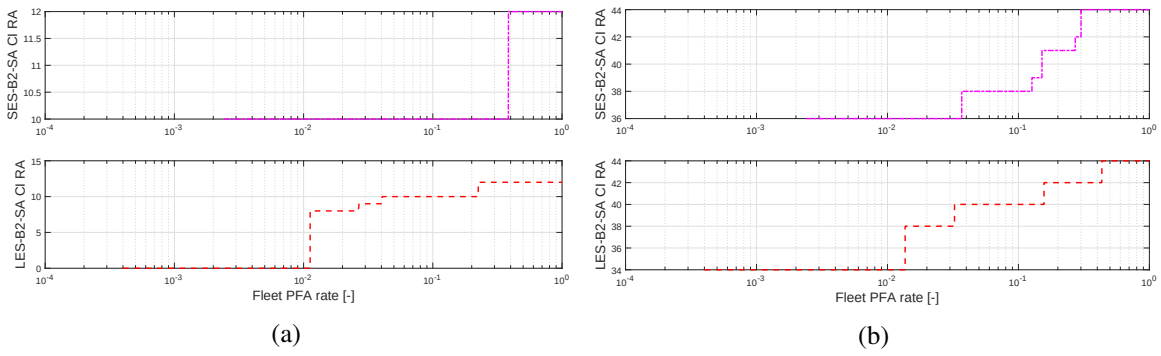

Figure 3 – Removal anticipation (RA) time in acquisitions vs. fleet false alarm rate for SES-SA (upper row, magenta dot-dashed) ad LES-SA (lower row, red dashed) indicators – a) Fault case number 1; b) Fault case number 2.

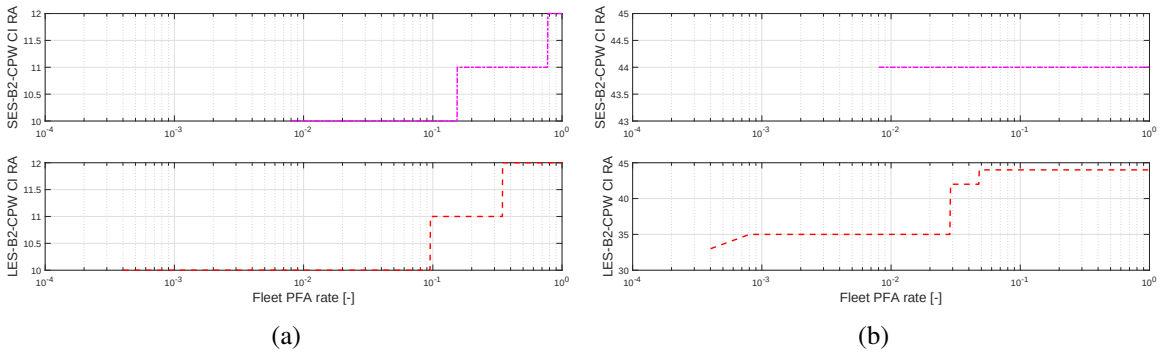

Figure 4 – Removal anticipation (RA) time in acquisitions vs. fleet false alarm rate for SES-CPW (upper row, magenta dot-dashed) ad LES-CPW (lower row, red dashed) indicators – a) Fault case number 1; b) Fault case number 2.

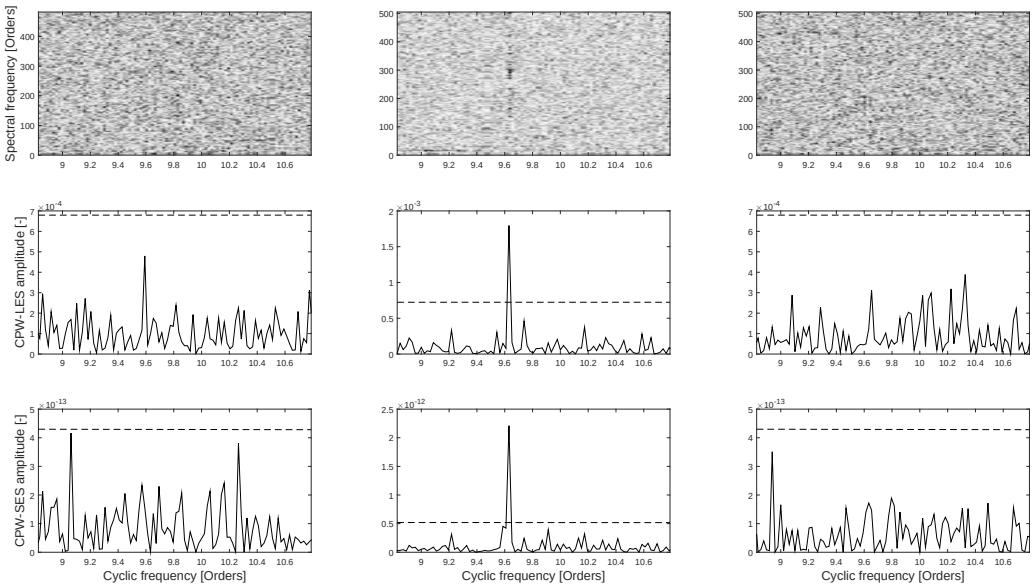

Figure 5 – Diagnostic charts for fault case 1. Upper row: cyclic coherence (darker areas corresponds to higher values); middle row: LES-CPW spectra; lower row: SES-CPW spectra. First column: healthy bearing; second column: detected outer race spalling; third column: gearbox replaced. Dashed line: 99.9 percentile threshold.

case, impacts will occur, exciting the bearing resonances and resulting in stronger CS2 symptoms with respect to those produced in case number 1, where the quasi-periodic change in the dynamic response is more likely due to the change of the load distribution within the contact line of the rolling elements rolling over the defective surface. As a matter of fact, the detection performance depends, among the other factors, from the evolution of the mechanical degradation. This does not appear to be the case for the ball bearing degradation, where the symptoms are of relatively comparable magnitude, despite the case number 3 presenting a more advanced degradation at the time of removal (figure 1). The fact that the contact taking place in ball bearings between the races and the elements can better be described as a point contact interaction could explain these results. In fact, any geometry of the degradation would almost surely provoke mechanical impacts between the elements and the race. The analysis of the diagnostic charts is an important step to confirm the alarms: the bearing fault signature presents itself as a clear cyclic excitation localized in the high spectral frequency band, and allows the analysts to reliably confirm whether the fault detection alert is effectively related to a mechanical fault. In fact, by observing the cyclic spectral coherence representation, it is possible in an operational scenario to rule out both the occurrence of false alarms and those false indications coming from corrupted measurements.

4.4 Impact of the operating conditions

In order to assess the sensitivity of the bearing monitoring indicators to the different operating conditions, the correlation of the indicator values to the torque and rotor speed values was studied. Figures 9 and 10 show such correlation for the LES-CPW outer race indicators related respectively to the roller (bearing 1) and to the ball bearing (bearing 2). Similar results were obtained for the other indicators, therefore only figures 9 and 10 were reported for brevity. As indicator value, the magnitude of the detected peak in the envelope spectrum was reported. This is a consistent indication, being the LES statistical distribution independent from the cyclic frequency. From the results, it can be observed that there is no significant correlation between the values of the indicator and the contextual parameter, whenever the indicator takes its nominal values. However, the higher values related to degraded conditions are mostly localized in correspondence of the high-torque region, for a rotor speed of around 97 percent of the nominal speed. This may indicate a slight sensitivity of the indicators to the operating conditions. However, it has to be pointed out that the majority of the recorded acquisitions occurred in the low rotor speed, high torque conditions. Being the acquisitions density in the region higher than in the rest of the operating spectrum, the likelihood of acquiring in those conditions during the progression of the fault is also higher. Finally, relatively high values of the indicator during the fault progression can be observed also in other regions of the operating spectrum, confirming its detection robustness to the different flying regimes of the helicopter.

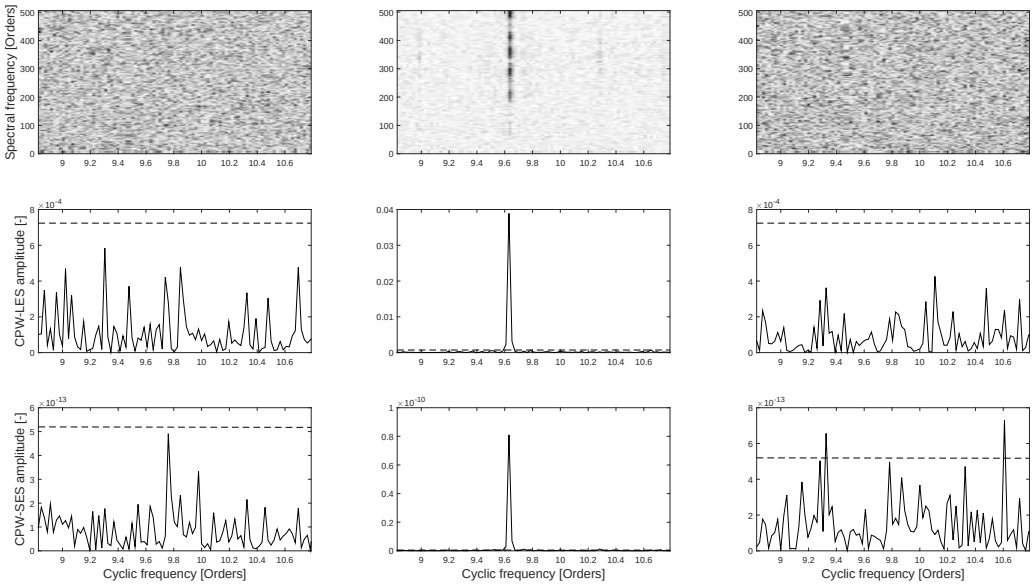

Figure 6 – Diagnostic charts for fault case 2. Upper row: cyclic coherence (darker areas corresponds to higher values); middle row: LES-CPW spectra; lower row: SES-CPW spectra. First column: healthy bearing; second column: detected outer race spalling; third column: gearbox replaced. Dashed line: 99.9 percentile threshold.

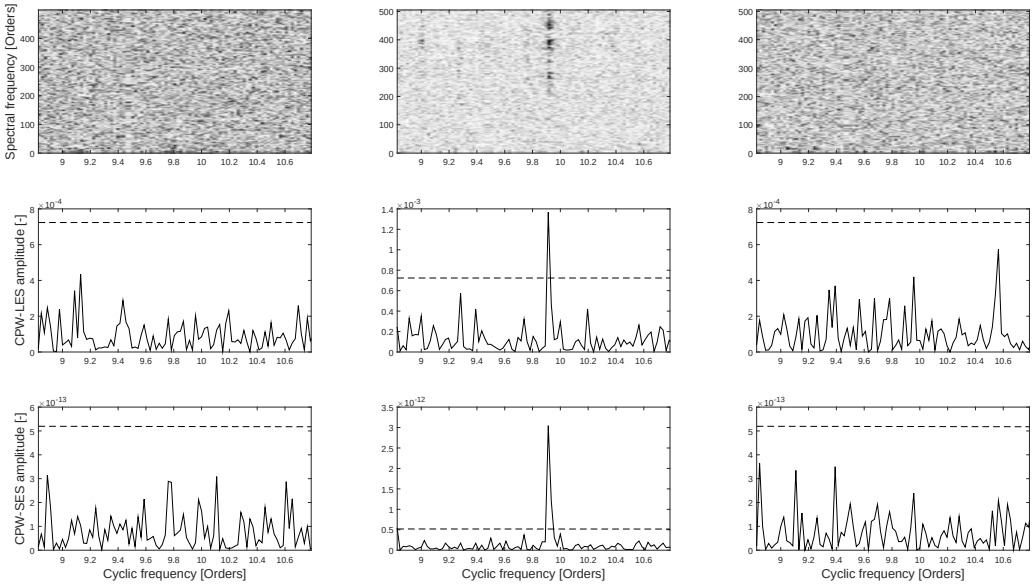

Figure 7 – Diagnostic charts for fault case 3. Upper row: cyclic coherence (darker areas corresponds to higher values); middle row: LES-CPW spectra; lower row: SES-CPW spectra. First column: healthy bearing; second column: detected outer race spalling; third column: gearbox replaced. Dashed line: 99.9 percentile threshold.

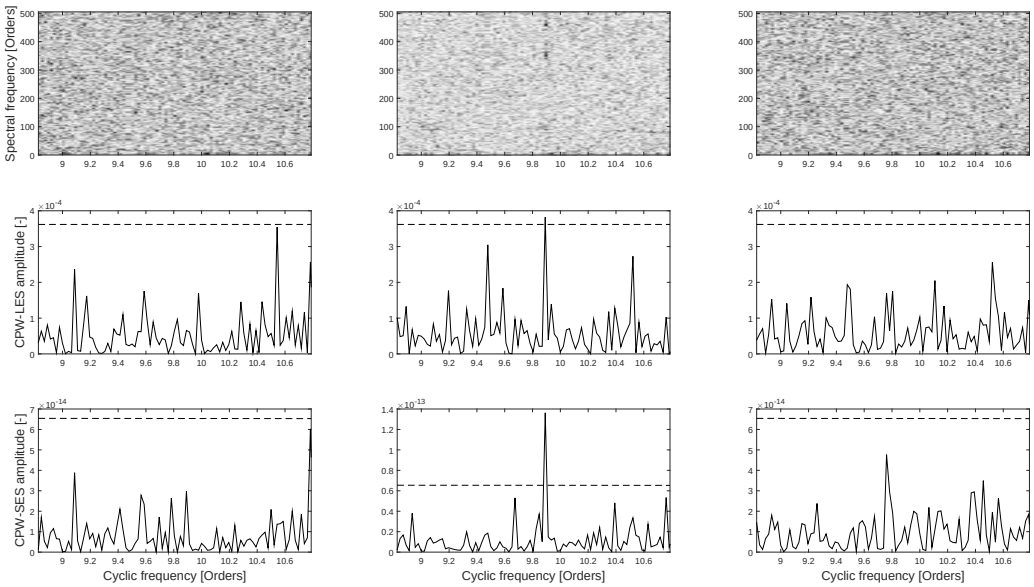

Figure 8 – Diagnostic charts for fault case 4. Upper row: cyclic coherence (darker areas corresponds to higher values); middle row: LES-CPW spectra; lower row: SES-CPW spectra. First column: healthy bearing; second column: detected outer race spalling; third column: gearbox replaced. Dashed line: 99.9 percentile threshold.

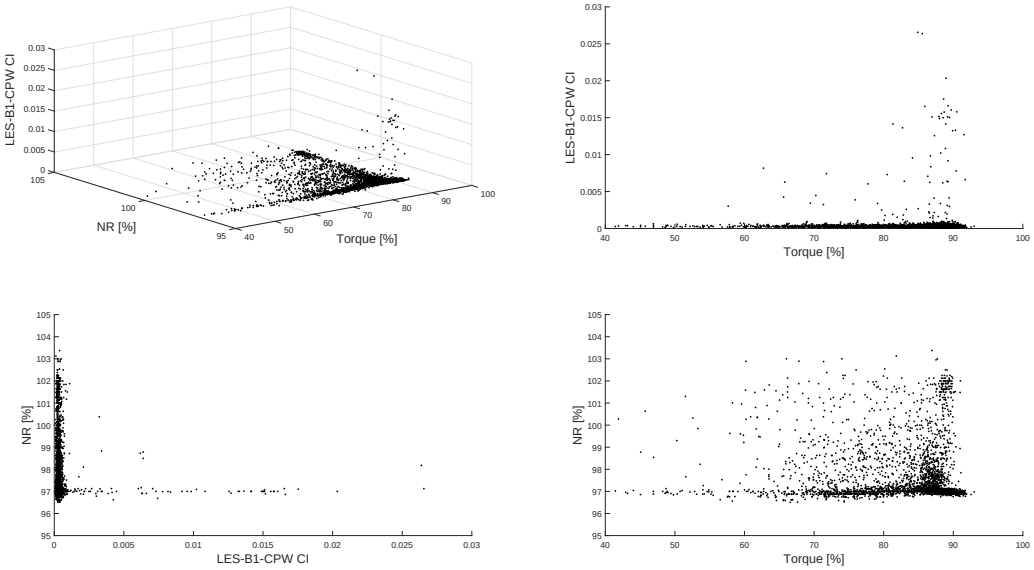

Figure 9 – Impact of the operating conditions on the bearing 1 outer race fault LES-CPW indicator values. Top-left: joint distribution of torque, rotor speed and indicator values; top-right: indicator values vs. torque; bottom-left: rotor speed vs. indicator values; bottom-right: rotor speed vs torque.

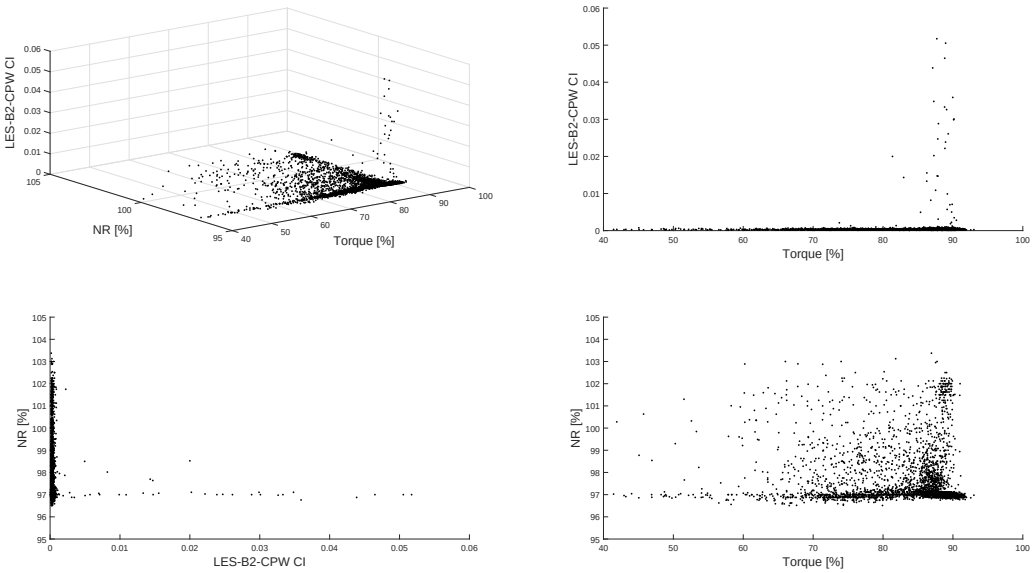

Figure 10 – Impact of the operating conditions on the bearing 2 outer race fault LES-CPW indicator values. Top-left: joint distribution of torque, rotor speed and indicator values; top-right: indicator values vs. torque; bottom-left: rotor speed vs. indicator values; bottom-right: rotor speed vs torque.

5 Conclusions

A predictive maintenance strategy for the monitoring of rolling element bearings in the context of helicopter operations was developed. The proposed methodology relies on a two-step fault detection and diagnosis process. The first step consists of devising reliable statistical indicators, allowing to attain a given false alarm rate. The second step consists of confirming eventual alarms through refined diagnostic analysis based on the estimation of the cyclic spectral coherence of the concerned signals. The devised procedure was validated on comprehensive, in-service helicopter fleet data set, comprising high-frequency acquisitions from fourteen machines flying according to several different profiles. Statistical indicators based on the logarithm envelope spectrum and on the squared envelope spectrum were compared in terms of both reliability in providing a given false alarm rate and ability to promptly anticipate four in-service bearing degradation cases. Two pre-processing algorithms based on synchronous average removal and cepstrum pre-whitening were considered, and some of their properties investigated. It was shown that indicators based on the logarithm envelope allow for a very fine tuning of the desired false alarm rate, together with providing acceptable detection performance in the considered cases. Conversely, squared envelope based indicators proved less reliable in actual operations. The results were shown to be consistent across the full range of considered operating conditions. The diagnostic step was shown to be able of accurately disclosing the faulty bearing signature, proving to be an effective discrimination mean to avoid unnecessary grounding of the machine in the occurrence of a HUMS alarm. At the same time, the burden of performing the diagnosis is restricted to those cases in which an alarm from the detection step actually occurs. The impact of different mechanical degradation shapes was also considered: it was shown that for the roller bearing outer race degradation cases, the fault shape has a significant impact on the HUMS detection performance. The developed approach allowed to deploy a statistically efficient, operationally valid procedure to monitor the rolling element bearings in helicopter mechanical transmissions within an in-service context, characterized by harsh mechanical environment, acquisition constraints and multiple different operating conditions. Remarkably, it could be used to deploy an effective, semi-automated monitoring for helicopter bearings which guarantees an effective condition based maintenance of the monitored components.

References

[1] A.R.S. Bramwell, D. Balmford, and G. Done. *Bramwell's helicopter dynamics*. Butterworth-Heinemann, 2001.

[2] A. Bayoumi et al. “Conditioned-Based Maintenance at USC-Part I: Integration of Maintenance Management Systems and Health Monitoring Systems through Historical Data Investigation”. In: *Proceedings of the AHS International Specialists Meeting on Condition Based Maintenance, Huntsville, AL*. 2008.

[3] B.D. Larder and M.W. Davis. “HUMS Condition Based Maintenance Credit Validation”. In: *American Helicopter Society 63rd Annual Forum*. 2007.

[4] B.D. Forrester. “Advanced vibration analysis techniques for fault detection and diagnosis in geared transmission systems”. PhD thesis. 1996.

[5] I. Howard. *A Review of Rolling Element Bearing Vibration Detection, Diagnosis and Prognosis*. Tech. rep. Defence Science and Technology Organization Canberra (Australia), 1994.

[6] R.J. Drago. *Fundamentals of Gear Design*. Butterworths, 1988.

[7] C. Capdessus, M. Sidahmed, and J.L. Lacoume. “Cyclostationary processes: application in gear faults early diagnosis”. In: *Mechanical systems and signal processing* 14.3 (2000), pp. 371–385.

[8] L. Bouillaut and M. Sidahmed. “Cyclostationary approach and bilinear approach: comparison, applications to early diagnosis for helicopter gearbox and classification method based on HOCS”. In: *Mechanical Systems and Signal Processing* 15.5 (2001), pp. 923–943.

[9] A.C. McCormick and A.K. Nandi. “Cyclostationarity in rotating machine vibrations”. In: *Mechanical systems and signal processing* 12.2 (1998), pp. 225–242.

[10] R.B. Randall, J. Antoni, and S. Chobsaard. “The relationship between spectral correlation and envelope analysis in the diagnostics of bearing faults and other cyclostationary machine signals”. In: *Mechanical systems and signal processing* 15.5 (2001), pp. 945–962.

[11] J. Antoni, J. Daniere, and F. Guillet. “Effective vibration analysis of IC engines using cyclostationarity. Part I: a methodology for condition monitoring”. In: *Journal of sound and vibration* 257.5 (2002), pp. 815–837.

[12] G.B. Giannakis. “Cyclostationary signal analysis”. In: *Digital Signal Processing Handbook* (1998), pp. 17–1.

[13] J. Antoni et al. “Cyclostationary modelling of rotating machine vibration signals”. In: *Mechanical systems and signal processing* 18.6 (2004), pp. 1285–1314.

[14] J. Antoni. “Cyclic spectral analysis of rolling-element bearing signals: Facts and fictions”. In: *Journal of Sound and vibration* 304.3-5 (2007), pp. 497–529.

[15] J. Antoni. “Cyclic spectral analysis in practice”. In: *Mechanical Systems and Signal Processing* 21.2 (2007), pp. 597–630.

[16] J. Antoni, G. Xin, and N. Hamzaoui. “Fast computation of the spectral correlation”. In: *Mechanical Systems and Signal Processing* 92 (2017), pp. 248–277.

[17] P.D. McFadden and J.D. Smith. “Vibration monitoring of rolling element bearings by the high-frequency resonance technique—a review”. In: *Tribology international* 17.1 (1984), pp. 3–10.

[18] P. Borghesani and M.R. Shahriar. “Cyclostationary analysis with logarithmic variance stabilisation”. In: *Mechanical Systems and Signal Processing* 70 (2016), pp. 51–72.

[19] P. Borghesani et al. “Testing second order cyclostationarity in the squared envelope spectrum of non-white vibration signals”. In: *Mechanical Systems and Signal Processing* 40.1 (2013), pp. 38–55.

[20] P. Borghesani and J. Antoni. “CS2 analysis in presence of non-Gaussian background noise–Effect on traditional estimators and resilience of log-envelope indicators”. In: *Mechanical Systems and Signal Processing* 90 (2017), pp. 378–398.

[21] P. Borghesani, P. Pennacchi, and S. Chatterton. “The relationship between kurtosis-and envelope-based indexes for the diagnostic of rolling element bearings”. In: *Mechanical Systems and Signal Processing* 43.1-2 (2014), pp. 25–43.

[22] J. Zeidler et al. “Adaptive enhancement of multiple sinusoids in uncorrelated noise”. In: *IEEE Transactions on Acoustics, Speech, and Signal Processing* 26.3 (1978), pp. 240–254.

[23] R.B. Randall and Y.J. Li. “Diagnostics of planetary gear bearings in the presence of gear vibrations”. In: *IMECHE Conference Transactions*. Vol. 5. Mechanical Engineering Publications. 1995, pp. 73–80.

[24] J. Antoni and R.B. Randall. “Unsupervised noise cancellation for vibration signals: part I—evaluation of adaptive algorithms”. In: *Mechanical Systems and Signal Processing* 18.1 (2004), pp. 89–101.

[25] J. Antoni and R.B. Randall. “Unsupervised noise cancellation for vibration signals: part II—a novel frequency-domain algorithm”. In: *Mechanical Systems and Signal Processing* 18.1 (2004), pp. 103–117.

[26] P.D. McFadden. “A revised model for the extraction of periodic waveforms by time domain averaging”. In: *Mechanical Systems and Signal Processing* 1.1 (1987), pp. 83–95.

[27] R.B. Randall, N. Sawalhi, and M. Coats. “A comparison of methods for separation of deterministic and random signals”. In: *International Journal of Condition Monitoring* 1.1 (2011), pp. 11–19.

[28] N. Sawalhi and R.B. Randall. “Signal pre-whitening using cepstrum editing (liftering) to enhance fault detection in rolling element bearings”. In: *Proceedings of the 24th international congress on condition monitoring and diagnostic engineering management*. 2011, pp. 330–336.

[29] P. Borghesani et al. “Application of cepstrum pre-whitening for the diagnosis of bearing faults under variable speed conditions”. In: *Mechanical Systems and Signal Processing* 36.2 (2013), pp. 370–384.

[30] J. Antoni and R.B. Randall. “The spectral kurtosis: application to the vibratory surveillance and diagnostics of rotating machines”. In: *Mechanical Systems and Signal Processing* 20.2 (2006), pp. 308–331.

[31] V. Camerini et al. “Impact of pulse time uncertainty on synchronous average: statistical analysis and relevance to rotating machinery diagnosis”. In: *Mechanical Systems and Signal Processing* 129C (2019), pp. 308–336.

[32] P.D. McFadden. *Interpolation techniques for the time domain averaging of vibration data with application to helicopter gearbox monitoring*. Tech. rep. AERONAUTICAL RESEARCH LABS MELBOURNE (AUSTRALIA), 1986.

[33] R.B. Randall and J. Antoni. “Rolling element bearing diagnostics—A tutorial”. In: *Mechanical systems and signal processing* 25.2 (2011), pp. 485–520.

[34] P.D. McFadden and J.D. Smith. “Model for the vibration produced by a single point defect in a rolling element bearing”. In: *Journal of sound and vibration* 96.1 (1984), pp. 69–82.

[35] P.D. McFadden and J.D. Smith. “The vibration produced by multiple point defects in a rolling element bearing”. In: *Journal of sound and vibration* 98.2 (1985), pp. 263–273.

[36] B.J. Hamrock and W.J. Anderson. *Rolling element bearings*. Tech. rep. 1983.

[37] R.B. Randall. “Applications of spectral kurtosis in machine diagnostics and prognostics”. In: *Key Engineering Materials*. Vol. 293. Trans Tech Publ. 2005, pp. 21–32.

[38] N. Tandon and A. Choudhury. “A review of vibration and acoustic measurement methods for the detection of defects in rolling element bearings”. In: *Tribology international* 32.8 (1999), pp. 469–480.

[39] J. Antoni and R.B. Randall. “A stochastic model for simulation and diagnostics of rolling element bearings with localized faults”. In: *Journal of vibration and acoustics* (2003).

[40] D. Ho and R.B. Randall. “Optimisation of bearing diagnostic techniques using simulated and actual bearing fault signals”. In: *Mechanical systems and signal processing* 14.5 (2000), pp. 763–788.

[41] J. Antoni and R.B. Randall. “Differential diagnosis of gear and bearing faults”. In: *Journal of Vibration and Acoustics* 124.2 (2002), pp. 165–171.

[42] S. Kass, A. Raad, and J. Antoni. “Self-running Fault Diagnosis Method for Rolling Element Bearing”. In: *Mechanism, Machine, Robotics and Mechatronics Sciences*. Springer, 2019, pp. 127–140.

[43] J. Antoni. “Cyclostationarity by examples”. In: *Mechanical Systems and Signal Processing* 23.4 (2009), pp. 987–1036.